Nondipole transitions at the 4*d* edges of Ta, Pt, and Au: Theory and experiment

A. Santoni*
Divisione Ingegneria dei Materiali, Comitato Nazionale per la Ricerca e lo Sviluppo dell'Energia Nucleare e delle Energie Alternative, Centro Ricerche Energia Casaccia, I-00100 Rome, Italy

A. Derossi†
Dipartimento di Fisica, Università di Trieste, via A. Valerio 2, I-34127 Trieste, Italy

P. Finetti
Sincrotrone Trieste Società Consortile perazioni, Padriciano 99, I-34012 Trieste, Italy

R. G. Agostino‡
Area per la Ricerca Scientifica e Tecnologica nella Provincia di Trieste, Padriciano 99, I-34012 Trieste, Italy

B. Luo§
Fritz-Haber-Institut der Max-Planck-Gesellschaft, Faradayweg 4-6, D-1000 Berlin 33, Germany
(Received 5 March 1992)

The 4*d* edges of Ta, Pt, and Au were measured by means of reflection-electron energy-loss spectroscopy for different primary-beam energies E_p in the maximum range $884 < E_p < 2186$ eV with the aim of investigating the nature of the electronic transitions involved at this edge. In order to allow a proper comparison of the measured edge intensities to each other, a normalization procedure was developed. On the basis of soft-x-ray-absorption spectroscopy data and by means of a theoretical muffin-tin generalized oscillator strength and differential cross-section calculations, it was possible to determine that nondipole *d*-*d* electron transitions are dominant at the 4*d* edges of all three elements. The observed edge-intensity decrease as a function of increasing atomic number is explained also on the basis of the amount of empty *d*-character states available at the Fermi level in each element.

I. INTRODUCTION

The investigation of unoccupied electron states by using synchrotron radiation photons as a source of excitation of core electrons has led in the past to the development of experimental techniques like extended x-ray-absorption fine-structure (EXAFS), near-edge x-ray-absorption fine structure (NEXAFS), and surface extended x-ray-absorption fine structure (SEXAFS), that have been recognized to be powerful tools for the investigation of the geometric and electronic structure of solid systems in the vicinity of the excited atoms.[1-6]

Considerable effects have also been devoted to the development of EXAFS-analog techniques, that are based on electron energy-loss spectroscopy (EELS) methods. These techniques make use of electrons as the primary excitation source and hence can be performed at a simple laboratory level. Important EELS-based structural techniques that provide EXAFS-like information are extended energy-loss fine structure[1,7,8] (EXELFS) and near-edge extended energy-loss fine structure (NEXELFS).[9] These require primary electron beams of the order of 100 keV and are bulk sensitive. Reflection-electron energy-loss spectroscopy (REELS) operated in a low primary electron energy range (500–2000 eV) is, on the other hand, surface sensitive[10] and therefore it has attracted considerable interest over the past years also because of its simplicity and the low-cost experimental setup.

The applicability of REELS-related techniques as an investigation tool able to provide EXAFS-like structural information was first demonstrated by De Crescenzi *et al.*, who developed the surface extended energy-loss fine-structure (SEELFS) method in the early 1980s.[11] Since then the SEELFS method was applied by several groups to the study of the local structure of metals,[11-13] semiconductors and insulators,[14,15] adsorbate systems,[16-18] clusters,[19] and interfaces.[20] Tyliszczack, Esposto, and Hitchcock also demonstrated the possibility of recording near-edge fine structures by means of REELS.[21] The energy-loss fine structures (EELFS) are usually detected above shallow edges where the binding energies of most of the systems of interest are a few hundred eV. In the framework of the EXAFS analysis, the Fourier transform of the EELFS oscillations yields a radial distribution function (RDF), whose most intense peak is directly related to the phase-shifted nearest-neighbor distance.[1,2] Phase shifts can be calculated theoretically and are known to allow the extraction of the correct crystallographic distances for the *K* and *L* core edges.[1,22] However, in the case of shallow *M* and *N* edges several discrepancies have been reported between calculated and experimentally determined phase shifts.[23] Several authors tried to explain the origin of such discrepancies over the past years. Central atom phase-shift calculations for dipole transitions were performed by Ekardt and Tran Thoai under different approximations,[24] but their results could not clarify the problem. Further empirical assumptions on the behavior of the

$p \rightarrow \varepsilon d / p \rightarrow \varepsilon s$ transition probability ratio as a function of the wave-vector by Tran Thoai and co-workers[13] led us to believe that neglect of the $\Delta l = -1$ dipole transition channel could have been responsible for the reported discrepancies. However, successive calculations performed by Combet Farnoux and Hitchcock[25] did not support that hypothesis. It is important to note that the above-mentioned tentative explanations were formulated within the framework of the dipole approximation. As the central atom phase shift depends on the symmetry of the final scattering state,[26] investigations on possible occurrences of dipole-forbidden transitions could shed new light on the problem.

Pioneer work by Meixner *et al.* and by Cazaux and Nassiopoulos[27] demonstrated years ago, on the basis of experimental data taken above the M_1 and $M_{2,3}$ edges, the taking place of nondipole transitions in Ni and a few years later Della Valle *et al.* reported on the possibility of such an occurrence.[28] Very recently Aebi *et al.*[29] convincingly demonstrated on the basis of extensive theoretical calculations and comparison with EELS data taken above the Cu 2*p*, 3*s*, and 3*p* edges that dipole selection rules are obeyed at some edges while other ones show dipole-forbidden transitions even at small momentum transfer. In following works by Luo and Urban the dependence of SEELFS oscillations above the Cu 3*p* (Ref. 30) and Pd 4*p* (Ref. 31) edges on the primary electron beam energy was studied in detail and the authors demonstrated with the support of theoretical generalized oscillator strength (GOS) calculations for the Cu 3*p* and Pd 4*p* edges the necessity of considering nondipolar transitions. They also clearly showed that in order to extract correct crystallographic distances from EXAFS data analysis of SEELFS oscillations the backscatterer phase shift must be calculated under the curved wave approximation (CWA) as first suggested by Tran Thoai and Ekardt for the 3*p* edges of Ni, Co, and Cu.[32] Although until now nondipolar channels have been observed only at shallow edges in Ni, Cu, and Pd, it is plausible to suppose that a similar behavior might be found in other materials. In fact, recent REELS measurements allowed the identification of dipole selection rule breakdown at the 3*d* edges of Pd and Rh.[33]

The aim of this work is to investigate the occurrence of nondipole transitions in a different row of elements: the 5*d* transition metals. We have performed REELS measurements at the 4*d* edges of Ta, Pt, and Au and studied the intensity of the edge jump as a function of different primary-beam electron energies. By means of the results obtained from theoretical muffin-tin *l*-projected GOS and differential cross-section calculations and by comparison x-ray-absorption spectroscopy (XAS) data, experimental REELS data give evidence of nondipole transitions occurring at the 4*d* edges of all the investigated metals. Furthermore, the edge jump intensities could also be correlated with the unoccupied density of states of each element.

II. THEORETICAL DETAILS

Following the theory of Bethe,[34] the cross section for an inelastic process between a fast electron and an atom from initial state nl (n is here the main quantum number and l the angular momentum) to the final state in the continuum $\varepsilon l'$ (ε is the energy, l' the angular momentum) can be expressed[34–35]

$$\frac{d\sigma_{nl,\varepsilon l'}}{dE} = \frac{4\pi a_0^2}{E_p \Delta E} \int_{q_{\min}}^{q_{\max}} \frac{df_{nl,\varepsilon l'}(q)}{dE} d\ln q^2 \,. \tag{2.1}$$

df/dE is the so-called generalized oscillator strength defined as

$$\frac{df_{nl,\varepsilon l'}(q)}{dE} = \frac{\Delta E}{q^2} \left| \int P_{nl}^*(\mathbf{r}) e^{i\mathbf{q}\cdot\mathbf{r}} P_{\varepsilon l'}(\mathbf{r}) d\mathbf{r} \right|^2 . \tag{2.2}$$

E_p and ΔE are here the primary energy of the incident electrons and the energy loss in rydbergs, respectively, and a_0 is the Bohr radius. q is the momentum transfer in units of a_0^{-1}. $q_{\min}$ and $q_{\max}$ are the minimum and the maximum momentum transfer, respectively, which are expressed by the primary energy E_p, the energy loss ΔE, and the maximal angle θ between the initial and the final directions of the incident electrons.

$$q_{\min} = (E_p)^{1/2} - (E_p - \Delta E)^{1/2} \,, \tag{2.3a}$$

$$q_{\max} = \{2E_p - \Delta E - 2[E_p(E_p - \Delta E)]^{1/2} \cos\theta\}^{1/2} \,. \tag{2.3b}$$

Since test differential cross-section calculations on Ta performed with $\theta = \pi$ and $\theta = \pi/2$ showed no appreciable difference, we used the value $\theta = \pi$ in our calculations.

As shown by Manson,[35] Eq. (2.2) for GOS can be developed to

$$\frac{df_{nl,\varepsilon l'}}{dE} = (2l+1)(2l'+1) \times \sum_{\lambda} (2\lambda+1) \left| \begin{bmatrix} l' & \lambda & l \\ 0 & 0 & 0 \end{bmatrix} \right|^2 \times \frac{\Delta E}{q^2} \left[\int_0^{\infty} P_{nl}^*(r) j_\lambda(qr) P_{\varepsilon l'}(r) dr \right]^2 . \tag{2.4}$$

j_λ is the spherical Bessel function of order λ.

$$\begin{bmatrix} l' & \lambda & l \\ 0 & 0 & 0 \end{bmatrix}$$

are the 3-j symbols.[38] $P_{nl}(r)$ is the radial part of the initial ground-state function $P_{nl}(\mathbf{r})$. It is given by the solution of the radial Schrödinger equation:

$$\left[\frac{d^2}{dr^2} + V(r) + \varepsilon_{nl} - \frac{l(l+1)}{r^2} \right] P_{nl} = 0 \,. \tag{2.5}$$

$V(r)$ is the atomic potential of Hartree-Slater type, which is tabulated by Herman and Skillman.[36] ε_{nl} is the energy of the electron in the nl-atomic ground state.

$P_{\varepsilon l'}(r)$ is the radial part of the continuum wave function which is also taken to be the solution of the radial Schrödinger equation:

$$\left[\frac{d^2}{dr^2} + V(r) + \varepsilon - \frac{l'(l'+1)}{r^2} \right] P_{\varepsilon l'} = 0 \,. \tag{2.6}$$

The potential $V(r)$ was calculated in terms of the self-energy by using the local density approximation and the plasmon pole approximation.[37] The numerical procedure follows that of Lundqvist.[39] By neglecting the imaginary part of the self-energy that describes the inelastic losses of the continuum waves, the effective potential $V(r)$ in Eq. (2.6) is given by

$$V(r)=\mathrm{Re}[M_0(k,k^2)]+V_0(r)$$
$$=\mathrm{Re}[M_0(k,k^2)]-\frac{2Z}{r}+\frac{2}{r}\int_0^r 4\pi r'^2\rho(r')dr'$$
$$+2\int_r^\infty 4\pi r'\rho(r')dr' \ . \quad (2.7)$$

$V_0(r)$ is the electrostatic potential. The self-potential $\mathrm{Re}[M_0(k,k^2)]$ and $V_0(r)$ can be calculated for a given electron density, which can be obtained by solving Eq. (2.5) for all bound electron states by using the Hartree-Slater potential.

The solid-state effect can be taken into account by a spherical average of the overlap of the atomic electron density. The muffin-tin radius was typically 0.75 times the first neighbor distance of the solid.

III. EXPERIMENT

In this work are shown synchrotron radiation data and REELS data. Soft-x-ray-absorption spectra were taken at the IBM U8B beamline at the National Synchrotron Light Source (vacuum ultraviolet ring) in Brookhaven. The U8B beamline consists of a switchable 6–10 m toroidal grating monochromator[40] equipped with a display-type electron spectrometer.[41] Partial yield x-ray-absorption spectra were recorded at the $4p_{3/2}$ and $4d$ Ta edges along with the current reference I_0 measured at the last refocusing mirror. For proper normalization, the I_0 divided Ta absorption spectra were further divided by an I_0 normalized absorption spectrum taken on a reference material over the same energy ranges. Copper was used as reference as it does not have any structure in the selected energy ranges.

The EELS experiments were performed in reflection mode at room temperature in a commercial Leybold-Heraeus apparatus equipped with an LH10 angle integrated (acceptance angle $\approx 12°$) hemispherical analyzer. The total pressure in the experimental chamber during data acquisition was better than 2×10^{-10} mbar. In order to further check the results, the measurement were also performed in normal incidence geometry in another system equipped with a single-pass Riber cylindrical mirror analyzer (CMA) and coaxial electron gun. As the second measurement run confirmed the previous results we shall describe and discuss here the first measurement run only.

High-purity polycrystalline samples of Ta, Pt, and Au were used. Surfaces were cleaned by Ar^+-ion etching and checked before and after each spectrum. Several sets of spectra were collected for each element and then added together to achieve good statistics.

Electrons were collected along the normal emission direction with the electron beam impinging onto the sample at 60° from the surface normal. Electron beam energies were set at 884, 1617, and 1946 eV for Ta, 1313, 1641, and 1989 eV for Pt, and 1473, 1844, and 2186 eV for Au. A further measurement at 2980 eV primary energy at normal incidence was performed on Ta in the CMA chamber.

The REELS measurements were taken in counting mode with the analyzer operating at 100 eV pass energy. Total experimental resolution measured at the elastic peak full width at half maximum (FWHM) turned out to be less than 2 eV. Constant resolution operation was necessary to record energy-loss spectra taken at different primary-beam energies with comparable resolution. This turns out to be useful when comparing normalized intensities.

In order to be able to perform an adequate data normalization (see below), the sample current was measured at the same time with the spectrum. As it is known that for a fixed electron gun emission current the measured sample current depends on the primary energy because of the different secondary electron emission efficiency, measurements were performed with a positively biased sample. The bias voltage was chosen to be 202 V for all the samples. Several measurement checks showed that at this bias voltage for the same electron gun settings the sample current was found to be independent of the primary-beam energies and the elements used in the experiment. Careful examination of the elastic peak with and without bias voltage did not show any changes and resolution degradation. The beam energies E_p listed above are therefore to be considered as total impact energies as they are obtained by adding the bias voltage to the primary energy.

As the aim of this study is also comparing the edge intensities measured at different primary energies with theoretical cross-section calculations, data normalization is required.

Because of the very low signal-to-noise ratio at the edges of interest, the electron gun current had to be set at a value too high to allow a simultaneous recording of the edge and the elastic peak without channeltron saturation. Therefore the usual normalization procedure, i.e., dividing the quantity of interest by the elastic peak height (or integral if the resolution is changing), is not applicable under these experimental conditions.

It also turned out to be impossible to normalize the data by simply dividing them by a straight line fitting the background before the edge[33] because for Ta, Pt, and Au the background height before the $4d$ edge is not independent from E_p but it was found to increase by increasing the impact energy.

For these reasons, a different normalization procedure was applied. The REELS data were taken together with the sample current reference at the optimum current settings. Separately, the elastic peak and its sample current reference were also recorded with the same settings as for the REELS data but with a lower target current in order to avoid channeltron saturation. In this way, by dividing the EELS data and their elastic peak by the corresponding current references it is possible to obtain data that are now independent from the excitation current. Now the current normalized data can be divided by the current

normalized elastic peak and hence a complete data normalization to the elastic peak can be obtained if, in the framework of the accepted two-step electron scattering model,[14] the possible difference of sample reflectivity values at the impact energies E_p and at the energies $E_p - \Delta E$, where ΔE are the 4d binding energies, is taken into account. According to other authors[42] the elastic scattering cross section $\sigma(E)$ for electrons with energies above 250 eV can be expressed as $\sigma(E) \propto E^{-a}$ with $0.5 < a < 0.75$. By fitting tabulated elastic cross sections for Ta and Au,[43] the value of a was estimated to be 0.55 for Ta and 0.51 for Au. Assuming the latter value also for Pt it is then possible to estimate the elastic scattering cross sections $\sigma(E)$ at the energies E_p and $E_p - \Delta E$ for all three elements. The elastic scattering cross sections at all the impact energies E_p used in the experiment turned out to be about 10% lower than the corresponding ones at the energies $E_p - \Delta E$ for all three elements. This indicates that all the measured edge intensities are overestimated by about 10%. This is a systematic error which does not affect the data much, since relative intensities remain unchanged.

This normalization procedure requires also that no variation of the other settings, such as, for example, the channeltron voltage and the electron gun spot-analyzer relative position, occurred during EELS data acquisition. This condition was easily fulfilled because te maximum data acquisition time per spectrum was about 50 min for Ta and about 2 h for Pt and Au and data were always taken with a well-stabilized electronics. This assumption was also confirmed by examination of several normalized elastic peaks taken at different times with the same settings. Reproducibility was good and the relative intensity variation was found in the worst case to be less than 7%. For these reasons we estimate the total error upper limit deriving from this normalization procedure to be abut 10%.

IV. RESULTS AND DISCUSSION

Figures 1(a) and 1(b) show the normalized and background subtracted 4d EELS spectra taken for Ta at 884, 1617, and 1946 eV, for Pt at 1313, 1641, and 1989 eV and for Au at 1473, 1844, and 2186 eV impact energy, respectively. At the lowest primary energies Ta and Pt $4d_{5/2}$ REELS edges showed a remarkable signal-to-background (s/b) ratio which was found to be 0.52% and 0.32% for Ta and Pt, respectively. The Au $4d_{5/2}$ edge s/b ratio was measured to be 0.12%.

The lowest impact energy values in the range used were chosen in order to ensure the validity of the first Born approximation[44] and all the other energies were chosen in order to obtain, where possible, similar momentum transfer values for all three elements. The $4d_{5/2}$ and $4d_{3/2}$ edge positions as measured at the edge inflection point turned out to be 314.6±0.3 and 331.5±0.3 eV for Pt in excellent agreement with tabulated data[45] and 336.0±0.3 eV for the Au $4d_{5/2}$, also in good agreement with photoemission binding energy values. As evidenced by derivative data, probably due to the superposition of multiple scattering structures, the Au $4d_{3/2}$ edge could not be resolved in the integral spectra. The Ta $4d_{5/2}$ and $4d_{3/2}$ edges were found at 228.0±0.3 and 239.8±0.3 eV, respectively. These values are about 2 eV higher than the tabulated binding energy (BE) ones. As explained below, this could be due to a density-of-states effect.

By fitting the measured 4d edges by means of a double-step function convoluted with a Gaussian-broadened Lorentzian information could be extracted on the intrinsic 4d core-hole lifetime broadening: this turned out to be 8.0±1.0 eV for Ta, about 6.0±1.0 eV for Pt, and 9.0±2.0 eV for Au. Calculated data give a broadening of about 7–8 eV for all three elements.[46]

From Fig. 1 it can be seen that Ta, Pt, and Au edge intensities show no appreciable dependence on the primary electron energy in the chosen range. Moreover, data also show that the edge intensities decrease with increasing atomic number. In fact, it is found that the Ta and Pt $4d_{5/2}$ edge normalized intensities are about 5.5 and 2.5 times, respectively, higher than the measured Au 4d edge normalized intensity.

In order to explain this behavior theoretical GOS and differential cross-section calculations were performed by employing a muffin-tin potential. The GOS results provided evidence of the occurrence of d-d transitions with a strength close to the edge (note that the zero of energy in

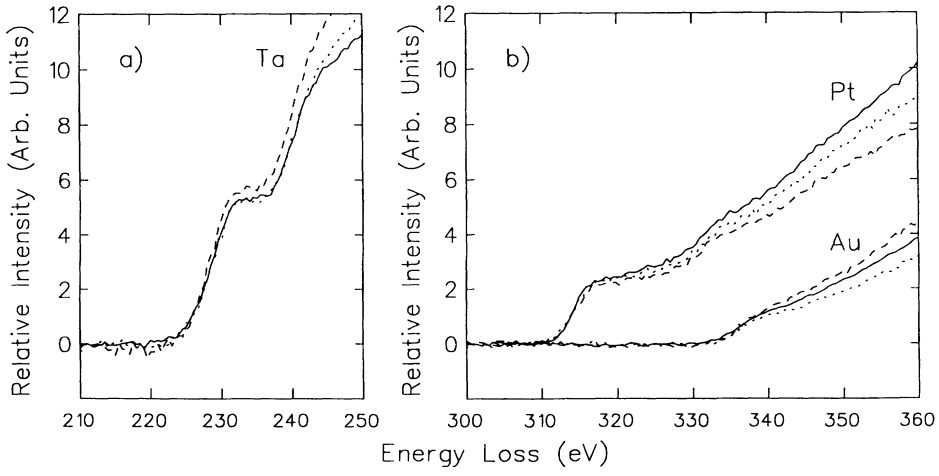

FIG. 1. (a) Ta 4d edge REELS spectra as obtained after normalization and background subtraction (see text) measured at 884 (full line), 1617 (dashed line), and 1946 eV (dotted line) impact energy, respectively. (b) Normalized and background subtracted (see text) Pt and Au 4d edge REELS spectra taken at different electron impact energies. Pt: 1313 (full line), 1641 (dashed line), and 1989 eV (dotted line). Au: 1473 (full line), 1844 (dashed line), and 2186 eV (dotted line).

the calculations corresponds to the vacuum level (E_v) higher than that obtained for d-p and d-f transitions for all three elements and for all three experimental primary-beam energies. Figure 2 shows the 4d initial-state GOS calculated for the lowest energy used for each element. GOS at the other energies provided similar results. The occurrence of dominating d-d transitions to the continuum can also be further evidenced by the results obtained from differential cross-section calculations. In Figs. 3(a), 3(b), and 3(c) the ratios $d\sigma^d/dE/\Sigma_l d\sigma^l/dE$, $d\sigma^p/dE/\Sigma_l d\sigma^l/dE$, and $d\sigma^f/dE/\Sigma_l d\sigma^l/dE$ calculated for 4d initial states at different primary energies for each element have been plotted as a function of the energy. Figures 3(a)–3(c) show that the d final-state differential cross-section relative contributions are higher than the p and f final-state ones for all three elements and for all three-primary energies. It is worth noting that as theory has shown that in Ta, Pt, and Au d-d transitions to the continuum can take place and are dominating at these momentum transfer values because of the favorable cross sections, it is reasonable to expect that the intensity at the edge can also be due to 4d-5d transitions and hence is proportional to the availability of empty electron 5d states. For these reasons we explain the remarkable intensities observed at the Ta, Pt, and Au 4d edges as mainly due to the occurrence of 4d-5d nondipole transitions.

This assumption is also supported by the density-of-states (DOS) structure of the investigated metals. DOS calculations[47] show a high d-projected density of unoccupied states above Fermi level for Ta and Pt. The same calculations show that there are no empty f states available at the Fermi edge (E_f) and the p-projected DOS above E_f is roughly more than a factor of 10 lower and nearly the same for the three elements.

It should be noted that also for Au the projected DOS configuration above Fermi level also shows, near the s and p states, free d states, according to the fact that Au is known to have hybridized d-character states.[48] As cross-section calculations predict dominating d-d transition also for Au [Fig. 3(c)], we are led to the assumption that the Au 4d edge intensity is also mostly proportional to the amount of available d-empty states.

By explaining the edge intensities in terms of nondipole d-d transitions, it could also be possible to explain the anomalous higher 4d edge energy positions found for Ta. In fact, unlike Pt that has a high d state density right at E_f, Ta DOS shows an appreciable density of free d states starting at about 2 eV above E_f with a high maximum at about 4.6 eV, thus shifting the density-of-states centroid to a higher-energy value.

Further experimental evidence on the occurrence of d-d nondipole transitions is provided by soft-x-ray-

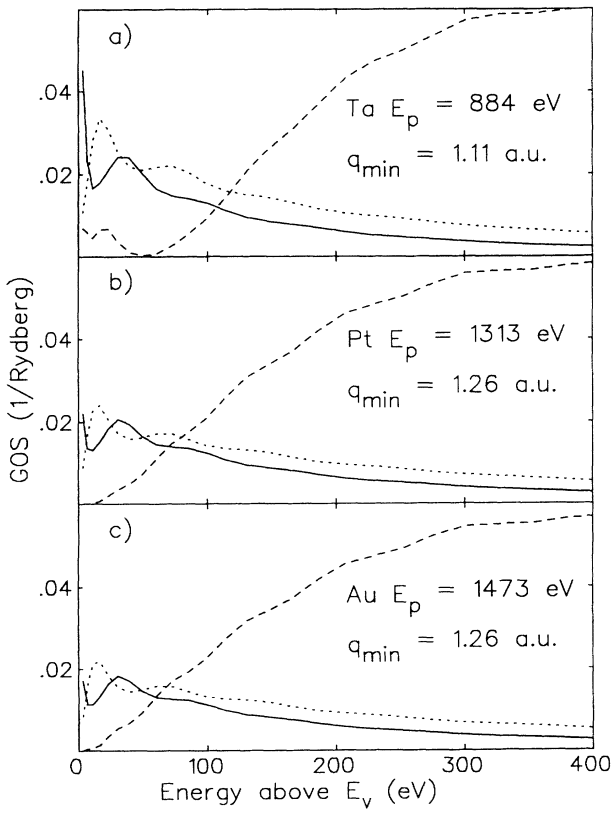

FIG. 2. 4d initial-state GOS calculated for different l final states: $l=1$ (dots), 2 (line), 3 (dash). For each element [(a), (b), and (c)] the GOS's were calculated for the minimum momentum transfer value (indicated in the figure) which corresponds to the energy indicated in each panel. E_v means vacuum level.

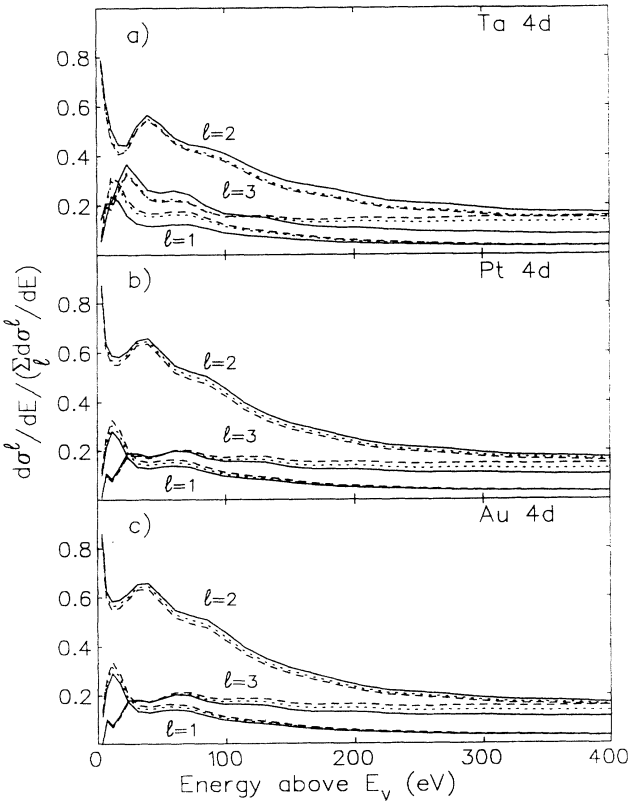

FIG. 3. 4d initial-state differential cross-section relative contributions calculated for different l final states ($l=1,2,3$) and different impact energies as a function of the energy above vacuum level (E_v). The sum over l was performed from $l=0$ to 5. For each l final state, full lines, dotted lines, and dashed lines correspond to the lowest, medium, and highest energy used for each element [(a), (b), and (c)], respectively.

absorption data measured at the Ta $4p_{3/2}$ and $4d_{3/2\text{-}5/2}$ edges. Soft-x-ray-excited transitions strictly obey dipole selection rules and on the basis of the symmetry character of the Ta DOS above Fermi edge[47] one would expect the 4*p* edge intensity to be higher than the 4*d* one. Figure 4 shows the absorption data taken at the Ta $4p_{3/2}$ [Fig. 4(a)] and 4*d* edges [Fig. 4(b)], respectively. As can be seen, the Ta $4p_{3/2}$ edge shows an appreciable *s*/*b* ratio at the edge while the Ta 4*d* edges are indistinguishable from the background. Analogously to the case of 4*d* metals where theoretical and experimental work[49] showed that *d*-*f* transitions take place several tens of eV above E_f, we tentatively explain the small intensity increase visible above the Ta $4d_{3/2}$ edge in Fig. 4(b) as possibly due to the onset of *d*-*f* transitions. The persistence of nondipole *d*-*d* transitions could be further evidenced in Ta at a higher electron primary-beam energy. Figure 5 shows the REELS spectrum of the Ta 4*d* edges taken at 2980 eV electron energy. The spectrum was collected at normal incidence in derivative mode with a CMA equipped with a coaxial electron gun. The *l*-projected ($l=1,2,3$) theoretical cross sections calculated for 2980 eV primary energy are shown in Fig. 5(b).

Theoretical calculations also show that the absolute values of the differential cross sections decrease for increasing primary energies in each of the three investigated elements. In the vicinity of the energy zero, calculations predict for Au and Pt a maximum intensity difference of about 27% in the total differential cross section between the lowest and the highest E_p used in the experiment, about 18% between the lowest and the middle energy, and about 11% between the medium and the highest energy. According to the previous sequence the percentage decrease in Ta is found to be 48%, 38%, and 16%, respectively. As already noted before, experimental edge jumps seem not to reflect the theoretical prediction as they showed to have within about 10% the same intensity for different E_p in all three elements. On the other hand, it is worth noting that, although reproducibility of experimental data would indicate an uncertainty well below 10%, allowing an error of about ±10% in the normalized intensities would account for the results obtained for Pt and Au. In case of Ta the maximum error bound is still not sufficient to explain the disagreement between theory and experiment in this case. For this reason we explain the discrepancy in the relative decrease of the edge intensity upon increasing of the primary energy as mainly due to the inaccuracy of the theoretical data close to the energy zero. In fact, as noted above, calculations take into account only unbound final states, thus neglect-

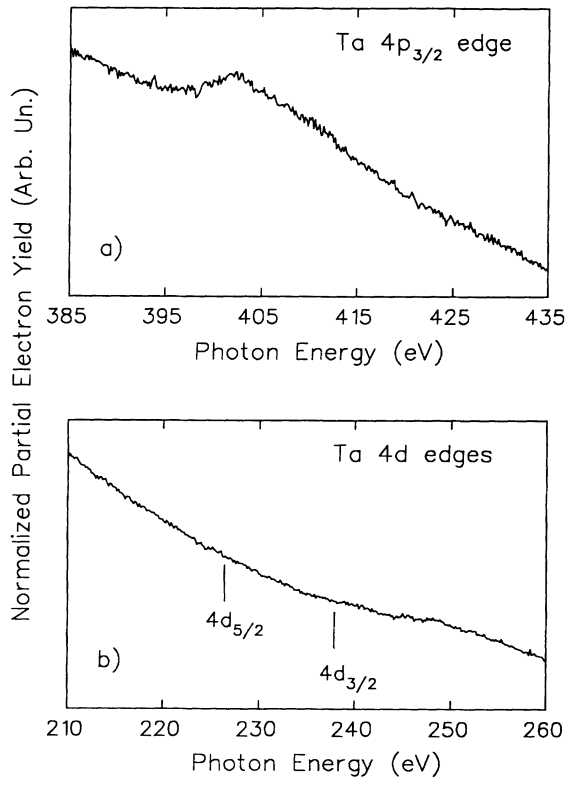

FIG. 4. (a) X-ray-absorption spectrum at the Ta $4p_{3/2}$ edge. The photon energy scale is calibrated within ±2 eV. (b) X-ray-absorption spectrum in the energy range of the Ta 4*d* edges. The energy positions of the Ta $4d_{5/2}$ and $4d_{3/2}$ edges are indicated in the figures. Uncertainty in photon energy calibration is ±1 eV.

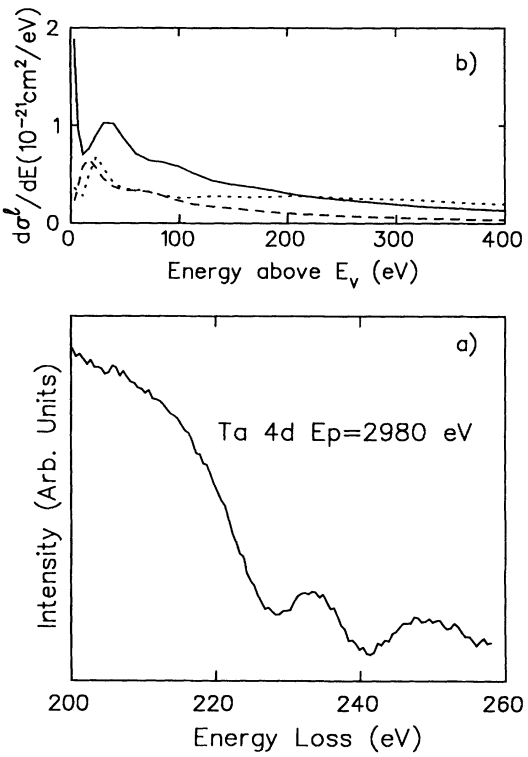

FIG. 5. (a) Ta 4*d* REELS spectrum taken in derivative mode with a CMA at 2980 eV primary energy. The two well-pronounced minima at about 228 and 240 eV correspond to the Ta $4d_{5/2}$ and $4d_{3/2}$ edges, respectively. Modulation was 3.5 V and acquisition time about 15 min. (b) Ta 4*d* initial-state differential cross sections as a function of the energy (E_v is the vacuum level) for different *l* final states calculated for 2980 eV primary energy. Full line: $l=2$; dashed line: $l=1$; dotted line: $l=3$.

ing the $4d$-$5d$ transition intensity which, as explained before, is expected to be strongly influenced by the density of states right above Fermi level. In addition, as pointed out in Sec. II, any other contributions to the edge intensity due to multiple scattering effects have not been accounted for by the present theoretical model.

The calculated differential cross sections are found to decrease with increasing atomic number and the Au total cross-section value in the vicinity of zero turned out to be on the average about 1.4 times and 4 times smaller than the values of Pt and Ta, respectively. These ratios are smaller than the experimental ones, which were measured to be about 5.5 and 2.5 for Ta/Au and Pt/Au, respectively. Therefore theoretical predictions reproduce only qualitatively the measured edge intensity decrease. As explained above, due to the inaccuracy of calculations in the vicinity of the energy zero, a quantitative comparison of the intensities between experiment and theory turns out to be unreliable.

V. CONCLUSIONS

The $4d$ edges of Ta, Pt, and Au have been measured for the first time by means of REELS, at different primary electron beam energies with the aim of investigating the nature of the electronic transitions which are involved at these edges. In order to compare edge intensities at different energies for the same element and among different elements a novel normalization procedure was developed. Theoretical calculations of GOS and differential cross sections performed for the investigated elements Ta, Pt, and Au at the experimental primary energies by employing a muffin-tin potential and comparison with soft-x-ray-absorption data have shown that, for all three elements and for all the primary energies used, the d-d nondipole transition is the dominating transition channel. The experimentally observed reduction of the edge intensity as a function of increasing atomic number was also found in agreement with calculations which predicted a cross-section decrease in going from Ta to Au. The discrepancy between the expected edge intensity ratios and the measured ones was explained by taking into account the amount of empty-d character states available in each element.

ACKNOWLEDGMENTS

The authors would like to thank the Laboratorio Tecnologie Avanzate Superfici e Catalisi (TASC) for making available the ESCA-Auger experimental chamber. Fruitful discussions with Professor C. Calandra, Professor S. Modesti, and Dr. F. J. Himpsel are gratefully acknowledged. Authors are also indebted to Professor E. Zeitler and Professor J. P. Urban for their interest and support in making the CMA system available and to S. Bartuschat and H. Junkes for helpful assistance. Research was carried out in part at the National Synchrotron Light Source, Brookhaven National Laboratory, which is supported by the U. S. Department of Energy, Division of Materials Science and Division of Chemical Sciences.

---

*Present address: European Synchrotron Radiation Facility, Boîte Postale 220, F-38043 Grenoble CEDEX, France

†Also at: Laboratorio Tecnologie Avanzate Superfici e Catalisi, Padriciano 99, I-34012 Trieste, Italy.

‡Present address: Dipartimento di Fisica, Università della Calabria, I-87036 Arcavacata di Rende, Italy.

§Present address: Max-Planck-Institut für Chemie, Postfach 3060, D-6500 Mainz, Germany.

[1]B. K. Teo and D. L. Joy, *EXAFS Spectroscopy, Technique and Application* (Plenum, New York, 1982).

[2]D. E. Sayers, E. A. Stern, and F. W. Lytle, Phys. Rev. Lett. **27**, 1204 (1971); E. A. Stern, D. E. Sayers, and F. W. Lytle, Phys. Rev. B **11**, 4836 (1975).

[3]F. W. Lytle, E. A. Stern, and D. E. Sayers, Phys. Rev. B **11**, 4825 (1975); P. A. Lee and J. B. Pendry, *ibid.* **11**, 2795 (1975).

[4]A. Bianconi, in *X-Ray Absorption: Principles, Applications Techniques of EXAFS, SEXAFS and XANES,* edited by D. Koningsberger and D. Prins (Wiley, New York, 1988).

[5]P. H. Citrin, P. Eisenberger, and R. C. Hewitt, Phys. Rev. Lett. **41**, 309 (1978).

[6]J. Stöhr, J. Vac. Sci. Technol. **16**, 37 (1979); J. Stöhr, L. Johansson, I. Lindau, and P. Pianetta, Phys. Rev. B **20**, 664 (1979); J. Stöhr, Z. Phys. B **61**, 439 (1985).

[7]J. J. Ritsko, S. E. Schnatterly, and P. C. Gibbons, Phys. Rev. Lett. **32**, 671 (1974).

[8]B. M. Kincaid, A. E. Meixner, and P. M. Platzman, Phys. Rev. Lett. **40**, 129 (1978).

[9]T. Lindner, H. Sauer, W. Engel, and K. Kambe, Phys. Rev. B **33**, 22 (1986).

[10]A. G. Nassiopoulos and J. Cazaux, Surf. Sci. **149**, 313 (1985).

[11]M. De Crescenzi, L. Papagno, G. Chiarello, R. Scarmozzino, E. Colavita, R. Rosei, and S. Mobilio, Solid State Commun. **40**, 613 (1981); M. De Crescenzi, G. Chiarello, E. Colavita, and R. Rosei, *ibid.* **44**, 845 (1982).

[12]M. De Crecenzi, G. Chiarello, E. Colavita, and R. Memeo, Phys. Rev. B **29**, 3730 (1984).

[13]A. Santoni, D. B. Tran Thoai, and J. Urban, Solid State Commun. **58**, 315 (1986); D. B. Tran Thoai, A. Santoni, W. Ekardt, and J. Urban, *ibid.* **58**, 319 (1986).

[14]M. De Crescenzi, L. Lozzi, P. Picozzi, S. Santucci, U. Benfatto, and C. R. Natoli, Phys. Rev. B **39**, 8409 (1989).

[15]A. Santoni, D. B. Tran Thoai, and J. Urban, Solid State Commun. **68**, 1039 (1989).

[16]A. Santoni and J. Urban, Solid State Commun. **63**, 257 (1987); Surf. Sci. **186**, 376 (1987).

[17]L. Papagno and S. Caputi, Phys. Rev. B **29**, 1483 (1984).

[18]M. De Crescenzi, F. Antonangeli, C. Bellini, and R. Rosei, Phys. Rev. Lett. **50**, 1949 (1983).

[19]M. De Crescenzi, M. Diociaiuti, P. Picozzi, and S. Santucci, Phys. Rev. B **34**, 4334 (1986); M. De Crescenzi, M. Diociaiuti, P. Picozzi, L. Lozzi, and S. Santucci, *ibid.* **35**, 5997 (1987).

[20]M. De Crescenzi, J. Derrien, E. Chainet, and K. Orumchian, Phys. Rev. B **39**, 5520 (1989).
[21]T. Tyliszczack, F. Esposto, and A. P. Hitchcock, Phys. Rev. Lett. **62**, 2551 (1989); T. Tyliszczack and A. P. Hitchcock, J. Vac. Sci. Technol. A **8**, 2552 (1990).
[22]B. K. Teo and P. A. Lee, J. Am. Chem. Soc. 101, 2815 (1979).
[23]For a review see M. De Crescenzi and G. Chiarello, J. Phys. C **18**, 3595 (1985).
[24]W. Ekardt and D. B. Tran Thoai, Solid State Commun. **45**, 1083 (1983).
[25]F. Combet Farnoux and A. P. Hitchcock, Solid State Commun. **64**, 961 (1987).
[26]See, for example, A. Messiah, *Quantum Mechanics,* 11th ed. (North-Holland, Amsterdam, 1985), Vol. I.
[27]A. E. Meixner, R. E. Dietz, G. S. Brown, and P. M. Platzman, Solid State Commun. **27**, 1255 (1978); J. Cazaux and A. G. Nassiopoulos, Surf. Sci. **162**, 965 (1985); A. G. Nassiopoulos and J. Cazaux, *ibid.* **165**, 203 (1986).
[28]F. Della Valle, G. Comelli, F. Zanini, R. Rosei, and G. Paolucci, Phys. Rev. B **38**, 13 355 (1988).
[29]P. Aebi, M. Erbudak, F. Vanini, D. D. Vvedensky, and G. Kostorz, Phys. Rev. B **41**, 11 760 (1990); **42**, 5369 (1990).
[30]B. Luo and J. Urban, Surf. Sci. **239**, 235 (1990).
[31]B. Luo, Ph. D. thesis, Freie Universität Berlin, 1990; B. Luo and J. Urban, J. Electron Spectrosc. Relat. Phenom. **57**, 399 (1991).
[32]D. B. Tran Thoai and W. Ekardt, Solid State Commun. **75**, 143 (1990).
[33]G. Paolucci, A. Santoni, G. Comelli, and K. C. Prince, Phys. Rev. B **44**, 10 888 (1991).
[34]H. A. Bethe, in *Quantentheorie,* edited by H. Geiger and K. Scheel, Handbuch der Physik Vol. 24/1 (Springer, Berlin, 1933).
[35]S. T. Manson, Phys. Rev. A **6**, 1013 (1972).
[36]F. Herman and S. Skillman, *Atomic Structure Calculation* (Prentice-Hall, Englewood Cliffs, NJ, 1973).
[37]P. A. Lee and G. Beni, Phys. Rev. B **15**, 2862 (1977).
[38]A. R. Edmonds, *Angular Momentum in Quantum Mechanics* (Princeton University Press, Princeton, NJ, 1957).
[39]B. I. Lundqvist, Phys. Kondens. Mater. **6**, 206 (1967).
[40]F. J. Himpsel, Y. Jugnet, D. E. Eastman, J. J. Donelon, D. Grimm, G. Langren, A. Marx, J. F. Morar, C. Oden, R. A. Pollack, and J. Schneir, Nucl. Instrum. Methods **222**, 107 (1984).
[41]D. E. Eastman, J. J. Donelon, N. C. Hein, and F. J. Himpsel, Nucl. Instrum. Methods **172**, 327 (1980).
[42]N. Masud, R. Baudoing, D. Aberdam, and C. Gaubert, Surf. Sci. **133**, 580 (1983); *Electron Diffraction 1927–1977,* Proceedings of the International Conference on Electron Diffraction, London, England, Sept. 1977, edited by P. J. Dobson, J. B. Pendry, and C. J. Humphreys, IOP Conf. Proc. No. 41 (Institute of Physics and Physical Society, London, 1978).
[43]M. E. Riley, C. J. McCallum, and F. Briggs, At. Data Nucl. Data Tables **15**, 443 (1975).
[44]M. Inokuti, Rev. Mod. Phys. **43**, 297 (1971); C. J. Powell, *ibid.* **48**, 33 (1976).
[45]*X-Ray Data Booklet,* edited by D. Vaughan, PUB-490 Rev., Lawrence Berkeley Laboratory (University of California, Berkeley, 1986).
[46]O. Keski-Rahkonen and M. O. Krause, At. Data Nucl. Data Tables **14**, 139 (1974).
[47]D. A. Papacostantopoulos, *Handbook of the Band Structure of Elemental Solids* (Plenum, New York, 1985).
[48]N. E. Christensen and B. O. Seraphin, Phys. Rev. B **4**, 3321 (1971); L. F. Mattheiss and R. E. Dietz. *ibid.* **22**, 1663 (1980).
[49]G. Paolucci, K. C. Prince, G. Comelli, A. Santoni, and O. Bisi, Phys. Rev. B **41**, 3862 (1990), and references therein.